JIG
JOURNAL OF IMAGE AND GRAPHICS

中国图象图形学报

主办：中国科学院遥感与数字地球研究所
中国图象图形学学会
北京应用物理与计算数学研究所

2013
08
VOL.18

ISSN1006-8961
CN11-3758/TB

数字文化遗产研究 P968

2013年8月 第18卷 第8期（总第208期）
中国图象图形学报
Zhongguo Tuxiang Tuxing Xuebao

目次

基于人脸五官特征的空域差错掩盖算法（第913页）

应用色彩空间聚类方法实现道路建模（第976页）

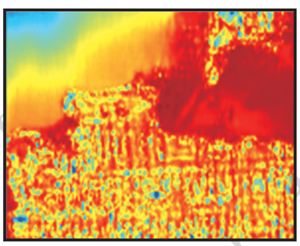

改进的基于非局部均值的极化SAR相干斑抑制（第1038页）

Volume 18, Number 8
Published August 16, 2013

CONTENTS

JOURNAL OF IMAGE AND GRAPHICS

Spatial error concealment algorithm based on the facial features (P913)

Road modeling using color spatial clustering (P976)

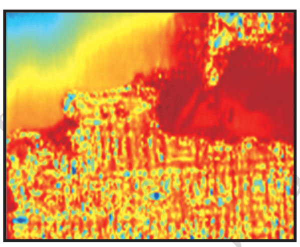

Improved polarimetric SAR speckle filter based on non-local means (P1038)

E-mail: jig@irsa.ac.cn
Website: www.cjig.cn
Tel: 010-64807995

中国图象图形学报
JOURNAL OF IMAGE AND GRAPHICS

中图法分类号: TP391.41　　**文献标识码**: A　　**文章编号**: 1006-8961(2013)08-1019-12

论文引用格式: Li Cuifang, Nie Shengdong, Wang Yuanjun, Sun Xiwen, Zheng Bin. Segmentation of sub-solid pulmonary nodules based on improved fuzzy C-means clustering[J]. 中国图象图形学报,2013,18(8):1019-1030. [DOI:10.11843/jig.20130817]

Segmentation of sub-solid pulmonary nodules based on improved fuzzy C-means clustering

Li Cuifang[1], Nie Shengdong[1], Wang Yuanjun[1], Sun Xiwen[2], Zheng Bin[3]

1. *Institute of Medical Imaging Engineering, University of Shanghai for Science and Technology, Shanghai* 200093, *China*;
2. *Radiology Department Shanghai Pulmonary Hospital, Shanghai*, 200433 *China*;
3. *Department of Radiology, University of Pittsburgh, Pittsburgh, PA* 15217-3025, *USA*

Abstract: Accurately and reliably automated segmentation of pulmonary tumors could play an important role in lung cancer diagnosis and radiation oncology. However, it remains a very difficult task in particular for segmenting pulmonary tumors associated with sub-solid nodules that are partially obscured in lung CT images. In this study, we propose and test an improved weighed kernel fuzzy C-means (IWKFCM) method that incorporates vessels structure information and classes' distribution as weights to segment sub-solid pulmonary nodules. For this purpose, a region of interest (ROI) of a nodule in center CT slice is manually defined. The IWKFCM algorithm is applied to identify and cluster the potential nodule pixels located in this manually-defined center slice and its adjacent (surrounding) slices. The sub-solid nodule is then segmented and defined through 3D connected component labeling and morphological post-processing. This segmentation method is tested using two datasets including 36 nodules selected from a public dataset (LIDC) and 18 nodules depicted on CT images collected from our local hospital. The average overlap ratios between the automated and radiologists' segmentation of nodules of two datasets are 76.18% and 71.65% respectively. In both datasets, the false-positive ratio (FPR) and false-negative ratio (FNR) are smaller than 17%. Experimental results show that the proposed method enables us to achieve more accurate result in segmenting sub-solid pulmonary nodules than the other previously reported clustering methods. The segmentation results could also provide a consultative reference for more accurately extracting image features and optimal classification of pulmonary nodules in developing computer-aided detection (CAD) schemes.

Key words: CAD; improved weighed kernel fuzzy C-means; sub-solid pulmonary nodule; 3D segmentation

改进的模糊聚类亚实质肺结节3维分割

李翠芳[1], 聂生东[1], 王远军[1], 孙希文[2], 郑斌[3]

1. 上海理工大学医学影像工程研究所, 上海　200093;
2. 上海市肺科医院影像科, 上海　200433;
3. 匹兹堡大学放射学系, 匹兹堡, 宾夕法尼亚州　15217-3025, 美国

摘　要: 肺癌是当今对人类健康与生命危害最大的恶性肿瘤之一。早期肺癌一般表现为肺结节,如能及时从肺部CT图像中检测到肺结节,便能及早发现肺癌,经治疗后可有效延长患者的生存时间,所以CT图像是肺癌诊断和疾

收稿日期:2012-07-03;**修回日期**:2012-12-14

基金项目:国家自然科学基金项目(60972122);上海市教委科研创新项目(09YZ216);上海市研究生创新基金项目(JWCXSL1102);上海市青年教师培养资助计划(slg11017)

第一作者简介:李翠芳(1987—　),女,2012年于上海理工大学获生物医学工程硕士学位,主要研究方向为医学成像技术及图像处理等。E-mail: 184975288@qq.com

通讯作者:聂生东,E-mail: nsd4647@163.com

中国图象图形学报
JOURNAL OF IMAGE AND GRAPHICS
Vol. 18, No. 8, Aug. 2013

病治疗的重要依据。但对全肺进行螺旋 CT 扫描产生的大量图像给人工检测肺结节带来了困难,因此,基于 CT 图像的肺结节计算机辅助检测(CAD)技术应运而生。由于 CAD 能有效辅助放射科医生提高肺结节的检测准确率与工作效率,降低漏诊与误诊率,因此,CAD 成了目前生物医学工程领域的研究热点之一。尽管目前报道的 CAD 系统所采用的方法各有不同,但基本上都是遵循以下步骤完成:1)CT 图像的预处理;2)肺结节的分割;3)特征提取及优化选择;4)肺结节的分类识别。其中对结节的精确分割与否直接影响到后续的特征选择与优化,而特征选择与优化又进而影响到分类器的分类属性,所以肺结节分割是基于 CT 图像的肺结节计算机辅助检测的关键步骤。

肺结节可细分为实质性结节(solid nodule)和亚实质性结节(sub-solid nodule)。其中完全屏蔽肺实质的结节称为实质性结节,否则称为亚实质性结节。实质性结节表现为边界比较规则的类圆形病灶,且密度较高、边界清晰,因此较容易分割,对实质性肺结节的分割国内外均有大量文献报道。与实质性肺结节相比,亚实质性肺结节其密度表现为磨玻璃影(GGO),且边缘不清晰(多带毛刺)、没有特定的形状。实质性结节中 93% 以上为良性病灶,而因为带有 GGO,亚实质性肺结节的恶性化程度较实质性结节而言表现得较高。因此,亚实质性结节的精确分割对发现早期肺癌更具应用价值,也面临更大的难度和挑战。

模糊聚类算法是一种基于模糊数学的常用的灰度图像分割方法,适合解决灰度图像中存在的模糊和不确定性问题。而经典的模糊聚类算法及其数种改进算法在聚类过程中具有明显的缺点和不足,仅考虑了每个像素的灰度值分别与各聚类中心的距离,未考虑相邻像素之间的影响及利用图像的空间信息,在分割时可能会丢失图像部分信息,所以不适用于亚实质性肺结节分割。针对肺 CT 图像中亚实质性肺结节的特点,对模糊 C 均值聚类(FCM)及其改进算法核模糊聚类(KFCM)和加权核模糊聚类(WKFCM)进行实践,提出一种改进的利用血管及类别结构信息加权的适用于亚实质肺结节的核模糊聚类(IWKFCM)3 维分割方法。该方法首先从肺 CT 序列图像的中心层中手动选取结节感兴趣区域(ROI),然后在由 ROI 临近层确定的 3 维感兴趣区域(VOI)内进行 IWKFCM 聚类,最后对聚类结果进行 3 维连通域标记及形态学处理得到最终结节的分割结果。本文分别采用 36 个 LIDC 标准数据和 18 个临床数据对所提出的分割方法进行评价,以放射科医生手动分割的区域作为金标准计算重合率,其均值分别为 71.65% 及 76.18%,且假阳性率及假阴性率均低于 17%。实验结果表明,相较于 FCM,KFCM 与 WKFCM 等未改进算法,IWKFCM 能够获得更准确的分割结果,并且分割效果同时优于目前文献报道的其他非模糊数学方法,为基于 CT 图像的肺结节计算机辅助检测提供了一种分割亚实质性肺结节的工具。

关键词: 计算机辅助检测;改进的加权核模糊聚类;亚实质肺结节;3 维分割

0 Introduction

Lung cancer is the leading cause of cancer death among people worldwide nowadays[1-2]. In the earlier stage, lung cancer generally exists in the form of pulmonary nodules. The size (or volume) of a nodule and its growth rate are an important criterion to differentiate between malignant nodules and benign ones. Since scientific evidences have shown that early detection of cancerous pulmonary nodules played a key role in improving a patient's chance for survival[3], accurately segmenting pulmonary nodules and measuring their volumes are important clinical tasks in lung cancer diagnosis as well as in the radiation oncology workflow to assess treatment efficacy. Computed Tomography (CT) is the most effective approach to detect and assess small pulmonary nodules[4]. However, the manual detection and segmentation of pulmonary nodules is very difficult and inefficient in the busy clinical environment due to the large amount of CT images. Therefore, it is necessary to develop a Computer-Aided Detection (CAD) system to help the radiologists read and assess CT images. A typical CAD scheme includes the following basic steps of image preprocessing: suspicious nodule segmentation, image feature extraction, and machine learning based classification[5]. Among them, nodule segmentation is a key step, since it determines the accuracy and reliability of the extracted image features and final classification results.

Pulmonary nodules can be briefly divided into solid and sub-solid categories. Solid nodules are often not obscured by the surrounding normal lung parenchyma, whereas sub-solid nodules are often obscured with relatively fuzzy boundary contours. In addition, the sub-solid nodules can also be classified as either partial-solid (a nodule with patches of parenchyma that are completely obscured) or nonsolid (a nodule with no such areas)[2], correspond to be named partial ground-glass opacity (GGO) and completed GGO for performing as GGO density. Usually, sub-solid nodules are more likely to be malignant than solid ones[6]. According to Nakata's respective statistic[7], the malignant rate was 93.3% (14 of 15 lesions) for partial GGO and 71.4% (20 of 28 lesions) for completed GGO.

Solid nodules are shown as a kind of circular lesions with regular shape, clear edges and high density, which is easy to segment, as shown in Fig. 1 (a). Many algorithms have been reported in the literature for solid nodule segmentation. Kostis et al. [8] proposed a method based on morphological operators, which mainly aims for solid nodule segmentation. It was tested on 18 nodules, and the overall performance was penalized by the poor performance of sub-solid nodules. de Hoop et al. [9] applied six commercially available semi-automated segmentation methods to 214 solid nodules between 3.3 mm and 30 mm in diameter. Sub-solid nodules have blurry edges and irregular shape (as shown in Fig. 1 (b) (c)), which made them more difficult to be segmented. Therefore, the segmentation of sub-solid nodules faces more challenges than the segmentation of solid ones. Only a few methods were developed and tested for segmenting sub-solid nodules. Zhang et al[10]. proposed a Markov random field (MRF) method with an adaptive intensity model, tested it on 21 pure or mixed GGNs and achieved an average overlap ratio of 0.69 ± 0.05. Zhou et al. [11] applied a nonparametric density estimation and likelihood map method for the segmentation of 10 clinical GGO nodules based on the measured image texture. It often fails when nodules are irregular and with weak edges. Yoo et al. [12] studied the indefinite and irregular boundary of a GGO and developed the deformable models to segment it. However, they did not make a quantitative assessment of the segmentation performance. Browder[13] developed a probability model based on nodules density distribution. When applying it to a test dataset with 20 nonsolid nodules, the mean overlap ratio between automated and manual segmentation was only 43%. Tao et al. [14] proposed a novel multi-level learning-based framework for automated detection and segmentation of GGOs in lung CT images. The reported average overlap rate in 20 nodules was 68% and the volume similarity was 86.5%. Meanwhile, more recent segmentation methods reported in the literature claimed to be able to handle nodules of different density types. Wang et al. [15] proposed a novel algorithm for segmenting pulmonary nodules on 3D CT images to improve the performance of CAD systems. Kubota et al. [16] developed an algorithm that was applicable to solid, non-solid and part-solid nodules and solitary, vascularized, and juxtapleural nodules. Both algorithms were tested on two datasets selected from the Lung Imaging Database Consortium (LIDC) library (http://imaging.cancer.gov/programsandresources/informationsystems/lidc) and achieved mean overlap ratios of smaller than 69%. Dehmeshki[17] presented an efficient algorithm to segment different types of pulmonary nodules by performing an adaptive sphericity oriented contrast region growing on the fuzzy connectivity map of the object of interest. The study reported that 84% of the segmented nodules were considered by the radiologist as acceptable while 16% segmented nodules were failed. Despite the great research effort, the performance of automated segmentation of sub-solid nodules in CT images is not satisfying and many technical challenges still remain.

Among many image segmentation methods, fuzzy clustering is one of the most commonly used[18]. Based on the fuzzy set theory, this data clustering method is very effective in addressing fuzzy and uncertain problem in gray images. However, when applied to image segmentation, only a few of traditional fuzzy clustering algorithms take the spatial information into account[19-21], thus most of those algorithms may lead to unexpected segmentation results. In this study, we propose an improved weight fuzzy kernel clustering method (IWKFCM) that considers both the structure and class information as weights. We then apply this improved data clustering method for the segmentation of sub-solid nodules, and make a comparative experiment with several conventional fuzzy clustering algorithms[22-24] to investigate its feasibility and performance.

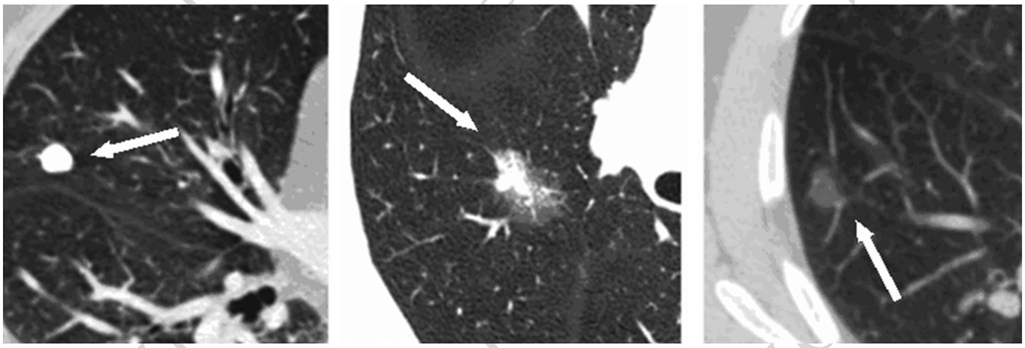

(a) A solid nodule (b) A partial-solid nodule (c) A nonsolid nodule

Fig. 1 Illustration of three nodules depicted on three CT image slices (as indicated by the white arrows)
图 1 各种不同类型的结节(白色箭头标识)

1 Methods

Due to the hazy appearance and the large overlap of intensity values between the sub-solid nodules and the surrounding vessels, a single and simple segmentation method often cannot produce acceptable results for segmenting sub-solid nodules. To achieve optimal segmentation results, we use a method based on fuzzy mathematics to cluster pixels involved in the sub-solid nodules. Specifically, we first investigate and compare the advantages and limitations of three popular data clustering methods, namely the fuzzy C-means (FCM), kernel fuzzy C-means (KFCM), and weighed kernel fuzzy C-means (WKFCM). We then develop a new method named improved weighed kernel fuzzy C-means (IWKFCM) aiming to optimally segment sub-solid pulmonary nodules. The new method considers vessels structure information and nodule classes' distribution as weights in the algorithm.

1.1 Related Work

1.1.1 FCM algorithm

In 1973 Bezdek proposed the FCM algorithm[22] and then FCM had been widely used in segmentation of gray images. FCM allows each pattern of the image to be associated with every cluster using a fuzzy membership function. In brief, suppose an image X contains n vectors, the object of FCM is to partition all vectors x_i $(i = 1, 2, \cdots, n)$ into c fuzzy clusters, and pursue objective function optimization to enable clustering center of each group minimum. According to fuzzy mathematical theory, each given point uses values between 0 and 1 as membership degree to determine the extent belonging to each group. Under the constraint of normalized provisions, the total sum of membership is equal to 1, expressing as

$$\sum_{i=1}^{c} u_{ij} = 1, j = 1, \cdots, n \tag{1}$$

where u_{ij} is the degree of membership of x_j in the cluster i, FCM aims to reach the minimization of the following objective function

$$J(U, c_1, \cdots, c_c) = \sum_{i=1}^{c} J_i = \sum_{i=1}^{c} \sum_{j=1}^{n} u_{ij}^m d_{ij}^2 \tag{2}$$

where m is a weighting exponent on each fuzzy membership and determines the amount of fuzziness of the resulting classification, $d_{ij} = \| c_i - x_j \|$ is the Euclidean distance between x_j and c_i, x_j is the *jth* of the image data, c_i is the center of the *ith* cluster, and d_{ij} is any norm expressing the similarity between any measured data and the center. Here, n represents the number of data and c represents the number of clustering centers. Fuzzy partitioning is carried out through an iterative optimization of the objective function shown above. The update of membership u_{ij} and the clustering centers c_i can be obtained by Lagrange theory, c_i and u_{ij} are shown as

$$c_i = \frac{\sum_{j=1}^{n} u_{ij}^m x_j}{\sum_{j=1}^{n} u_{ij}^m} \tag{3}$$

$$u_{ij} = \frac{1}{\sum_{k=1}^{c} \left(\frac{d_{ij}}{d_{kj}}\right)^{2/(m-1)}} \tag{4}$$

This iteration will stop when $\max\{|u_{ij}^{(t+1)} - u_{ij}^t|\} < \varepsilon$, where ε is a termination criterion between 0 and 1, and t is the iteration step. The classic FCM algorithm only considers the gray level during clustering process when using it for image segmentation. Since no spatial information is taken into account, FCM would lead to unexpected results of segmentation when dealing with the images corrupted by noises or complex images with fuzzy properties. For example, when applying FCM to pulmonary nodules corrupted by image noises, parts of the weak edge in some nodules are unable to be correctly segmented.

1.1.2 KFCM algorithm

To improve the separability or discriminatory power of the clustering segmentation algorithm on the input data in different classes (i. e., the sub-solid no- dules and normal lung structures in this study), a kernel function is usually applied to classic FCM. The kernel function can be used to implicitly map the input image data to a potentially higher dimensional inner product space without knowing the exact mapping function[23]. KFCM is a fuzzy clustering in high-dimensional feature space by using an implicit non-linear function. It transforms the nonlinear clustering problem to a linear one. The objective function of KFCM algorithm is shown as

$$J = \sum_{i=1}^{c}\sum_{j=1}^{n} \mu_{ij}^m \| \Phi(x_j) - \Phi(c_i) \|^2 \tag{5}$$

where Φ is an implicit non-linear mapping function. A Gauss RBF function is commonly selected as kernel function in this field. For the Gauss RBF kernel function, the Euclidean distance can be rewritten as

$$\begin{aligned}\| \Phi(x_j) - \Phi(c_i) \|^2 &= K(x_j, x_j) + K(c_i, c_i) - \\ &2K(x_j, c_i) = 2 - 2K(x_j, c_i)\end{aligned} \tag{6}$$

where $K(\,,\,)$ denotes the Gauss RBF kernel function.

We can get the updated values of membership degree and clustering centers by using the Lagrange constraint condition. It is easy to achieve this iteration like FCM.

Compared with the classic FCM, KFCM can detect more complete edge information when it is used in nodule segmentation. But, KFCM also establishes the objective function only based on gray information of an image and neglects the information included in the pixel position and the distribution about clusters. This clustering process generally cannot effectively distinguish the small object from background in images and may lead to incomplete segmentation. The interference from small object may be large. It may lead to errors in the recognition of vessels in clustering results. Besides considering the separability of input data in high dimension feature space on clustering influence, structure information of the pixels should also be introduced to the partition process, so as to obtain more accurate separation of background and object.

1.1.3 WKFCM algorithm

The KFCM algorithm does not include information about the distribution of clusters. It is still not an optimal algorithm when the fuzziness level of the input data in the same class (e. g., pixels inside a sub-solid nodule) is relatively high. The small class may be misclassified or merged into big class during KFCM clustering when they are extremely different. In order to solve this problem, an improved KFCM was proposed in Xue's research[24]. An additional weighting factor is assigned to each class in this algorithm, which represents the importance of the cluster classes. When the class has dense distribution with more elements, it is more important and the memberships of its elements are also larger. Additionally, conversely elements of a smaller class have more sparse distribution, so it is less important than the former. The new objective function of WKFCM is expressed as

$$J = \sum_{i=1}^{c}\sum_{j=1}^{n} a_i \mu_{ij}^m \| \Phi(x_j) - \Phi(c_i) \|^2 \tag{7}$$

where the class weight a_i meet constraint conditions: $\sum_{i=1}^{c} a_i = 1$. Based on this improvement, Xue got better performance when using the algorithm on general brain MRI-T1 image segmentation.

However, comparing the segmentation results of applying FCM, KFCM, and WKFCM to the same nodules, the vessels in lung CT images greatly interfered in nodule segmentation and it is one of the primary reasons leading to generate false positive results. Since the surrounding high-intensity vessels have similar grayscale to the sub-solid nodules, finding an accurate separation boundary is difficult and often result in incomplete segmentations. It would be helpful to consider adding the effective spatial constraints into the objective function.

1.2 Improved weighed kernel fuzzy C-means based on structure and classes information

Due to hereinbefore consideration, we proposed IWKFCM based on vessels structure and classes information to improve or modify the WKFCM[24]. Specifically, in IWKFCM algorithm, weight ω_j associated with vessel structure is added into the objective function of the WKFCM algorithm,

$$J = \sum_{i=1}^{c} a_i \sum_{j=1}^{n} \omega_j \mu_{ij}^m \| \Phi(x_j) - \Phi(c_i) \|^2 \quad (8)$$

Based on the membership of the normalization and category weight constraints to minimize the objective function J, we obtain

$$\mu_{ij} = \frac{a_i(1 - K(x_j, c_i))^{-1/(m-1)}}{\sum_{i=1}^{c} a_i(1 - K(x_j, c_i))^{-1/(m-1)}} \quad (9)$$

$$c_i = \frac{\sum_{j=1}^{n} \omega_j \mu_{ij}^m K(x_j, c_i) x_j}{\sum_{j=1}^{n} \omega_j \mu_{ij}^m K(x_j, c_i)} \quad (10)$$

$$a_i = \frac{\sum_{j=1}^{n} \omega_j \mu_{ij}^m (1 - K(x_j, c_i))}{\sum_{i=1}^{c} \sum_{j=1}^{n} \omega_j \mu_{ij}^m (1 - K(x_j, c_i))} \quad (11)$$

In Eq. (11) the class weight α_i is a dynamic value and can be adjusted automatically during the clustering process according to different types of nodules. For the calculation of vessels weight we adopt Frangi's work[25] that proposed a multi-scale vesselness measure to assign a value from 0 to 1 to each pixel of an image. This assigned value reflects the confidence of a point being a vessel pixel. In 3D images, for a single scale σ, a response at a point x is calculated as

$$V_\sigma(x) = \begin{cases} 0 & \lambda_2 \geqslant 0 \text{ or } \lambda_1 \geqslant 0 \\ (1 - e^{-\frac{R_a^2}{2\alpha^2}}) e^{-\frac{R_b^2}{2\beta^2}} (1 - e^{-\frac{S^2}{2\gamma^2}}) V_F & \text{else} \end{cases} \quad (12)$$

where $R_a = \frac{|\lambda_2|}{|\lambda_1|}$, $R_b = \frac{|\lambda_3|}{\sqrt{|\lambda_2 \lambda_1|}}$, $S = \sum_{i \leqslant 3} \sqrt{\lambda_i^2}$, $V_F = e^{-\frac{2c^2}{|\lambda_2| \lambda_3^2}}$, λ_i s are eigenvalues of the Hessian matrix and α, β, γ are constant normalization factors. R_a differentiates between plate and line like structures, R_b accounts for deviation from a blob like structure, and S differentiates between foreground (vessel) and background (noise). In order to keep the n^{th}-order derivatives of the vesselness function, a smoothness factor V_F is multiplied with a constant c. The vesselness function is calculated at multiple scales[26], and the maximum response is selected for vesselness measure calculation. As shown in Fig. 2(c), Frangi's method is able to recognize blood vessels.

To introduce vessel weights into our algorithm, ω_j is defind as

$$\omega_j = \frac{|1 - V(x_j)|}{\sum_{j=1}^{n} |1 - V(x_j)|} \quad (13)$$

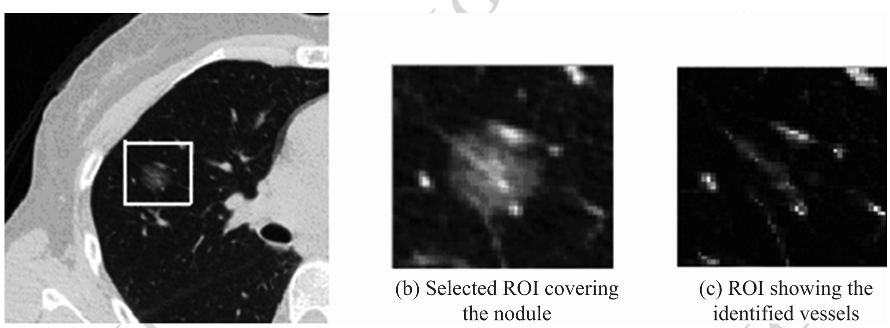

(a) A section of CT image slice involving the targeted nodule

(b) Selected ROI covering the nodule

(c) ROI showing the identified vessels

Fig. 2 An example including the illustration

图2 ROI选取及血管权值

Through this normalization, vessel weight is determined. As a result, during the image data clustering process, our algorithm automatically assign smaller weight values where there are vessels and higher weight values where there are no vessels. By introducing the vessel structure information about the pixels, the disturbance of blood vessels in nodule segmentation can be decreased.

2 Segmentation of sub-solid pulmonary nodules using IWKFCM

To segment a pulmonary nodule, IWKFCM algorithm consists of the following image processing steps (as shown in Fig.3). First, a region of interest(ROI) covering a 3D nodule is manually selected and determined in the center CT slice where the observer estimates the nodule having the largest section (size). Second, IWKFCM is applied to clustering pixels within the ROI. Third, the algorithm detects a sub-solid nodule mask through 3D connected component labeling and morphological post-processing.

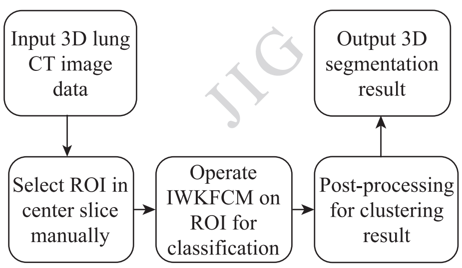

Fig. 3 A flow chart showing the steps of segmenting 3D pulmonary nodules using the proposed method

图 3 亚实质肺结节 3 维分割算法流程

2.1 Select ROI

We first select a ROI with a square in the center slice of 3D lung CT images. Using the manually selected ROI as a seed, the computer scheme then automatically expands it to the adjacent surrounding slices (in front and behind the selected center slice) to define a cube volume containing the entire nodule namely a volume of interest (VOI). The selection of ROI helps narrow the data clustering area and reduce vessels and other tissues interference (as shown in Fig. 2(b)).

2.2 Clustering using IWKFCM

After determining a data clustering VOI, IWKFCM is applied to conduct data clustering. The key to run IWKFCM is to decide the predetermined clustering numbers, which is known to partition the data into several categories. The number of clusters will directly affect the clustering quality of the image data. Using the same classes defined by Xiang et al[27], we divide lung CT images into three categories namely, 1) nodule and vessel, 2) lung cavity, and 3) background.

2.3 Post-processing using 3D connected component labeling and morphological techniques

After IWKFCM data clustering, some small background elements that have similar grey level distribution as the nodules remain in each determined VOI, which may include some interference points of the vessels. Attached vessels can be easily identified and removed through 3D connected component labeling and basic morphological methods including erosion and dilation operations. Morphological methods can remove noise, and isolate individual elements or join disparate elements in an image through finding intensity bumps or holes in an image.

3 Experimental results

3.1 Two testing image datasets

To evaluate the performance of our proposed pulmonary nodule segmentation method, two datasets are selected and used in this study. One is selected from a publically available dataset downloaded from Lung Imaging Database Consortium (LIDC) library and one is selected from the CT examinations acquired from a local hospital.

LIDC is a cooperative effort launched by the National Institutes of Health, USA, in 2000, aiming to construct a set of annotated lung images, especially low-dose helical CT scans of adults screened for lung cancer, and related technical and clinical data, for the development, testing, and evaluation of different computer-aided cancer screening and diagnosis technologies[28]. LIDC library includes two datasets. LIDC1 has 23 sets of CT examination data, while LIDC2 has accumulated more than 400 CT examinations and these examination were all blindly read by up to four radiologists independently who annotated locations and characteristics of nodules and provided manual segmentations for those that are considered larger than 3 mm in diameter. The results of the blind reads were collected and the same radiologists unblindly read the cases again with segmentations of the other radiologists. Hence, we use the provided manual segmentation results as the "truth" or reference to assess the performance of the automated schemes. We select 36 sub-solid nodules from LIDC2, including 13 non-solid and 23 partial-solid ones for this study. These nodules depicted on the CT image slices with thickness varying from 0.6 mm to 3mm. The diameters of nodules range from 3 mm to 19 mm, with an average value of 9.75 mm. Image matrix for all CT slices is 512 × 512 pixels.

The second dataset includes 18 sub-solid pulmonary nodules depicted on the images of clinical CT examinations conducted in Shanghai Pulmonary Hospital using a Philips 40-Row spiral CT scanner. All images have a matrix of 512 × 512 pixels with 2.0 mm slice thickness and 12 bit image depth. The spatial resolution of CT images ranges from 0.683 6 mm to 0.799 3 mm. Among the 18 detected nodules, 12 are identified as non-solid and 6 are partial-solid nodules. The diameters of nodules range from 6 mm to 26 mm, with an average value of 12.5 mm. The boundary of each nodule is manually segmented and marked by the radiologists from Shanghai Pulmonary Hospital. All segmentation results are verified by a senior radiologist. The recorded manual segmentation results are also used as the "truth" or the comparison reference in this study to assess performance of the automated segmentation schemes.

3.2 Performance evaluation criteria

A number of evaluation methods and criteria have been previously reported in the literatures for evaluating performance of automated nodule segmentation. The most popular method is to compare automated segmented nodule boundary contour with the radiologist's manual segmentation which is considered as boundary ground truth markings of the nodules. For this purpose, an overlap ratio was used as evaluation criterion[10]. In this study, we adopt the definition of overlap ratio used in references[13-16]. We compute two overlap ratios (also named Jaccard Ratio or Jaccard index) of 1) the entire pulmonary nodule volume of all involved slices (*Overlap*, evaluate it in 3D volume structure), 2) the pulmonary nodule area depicted on center slice (*Overlap_CS*, evaluate it in 2D planar domain). Jaccard Ratio is a statistic used for comparing the similarity and diversity of sample sets. It measures similarity between sample sets, and is defined as the size of the intersection divided by the size of the union of the sample sets. Assuming $\boldsymbol{S}$ as the area segmented by the automated schemes, while $\boldsymbol{T}$ representing the reference area defined by radiologists, the Jaccard Ratio over the entire pulmonary nodule volume is then expressed as

$$Overlap = \frac{|\boldsymbol{S} \cap \boldsymbol{T}|}{|\boldsymbol{S} \cup \boldsymbol{T}|} \tag{14}$$

In addition to these two overlap ratios, we also compute the other two performance assessment indices namely False Positive Ratio (FPR) and False Negative Ratio (FNR), as used in pulmonary nodule segmentation result validation[29]. FPR represents the rate of false positive area in segmentation results as comparing to the reference segmentation area provided by radiologists; similarly FNR is the rate of false negative area as comparing to the reference area, as shown in Fig. 4. TN, TP, FN, FP is correspondingly short for True Negative, True Positive, False Negative, False Positive. In general, FPR represents over-segmentation and FNR indicates under-segmentation. Hence, both FPR and FNR can be useful to evaluate different types of segmentation errors. They are respectively defined as

$$\mathrm{FPR} = \frac{|\boldsymbol{S} - \boldsymbol{T}|}{|\boldsymbol{T}|} \tag{15}$$

$$\mathrm{FNR} = \frac{|\boldsymbol{T} - \boldsymbol{S}|}{|\boldsymbol{T}|} \tag{16}$$

3.3 Experimental results

Fig. 5 shows a complete example of the segmentation process applying to one nodule using FCM, KFCM, WKFCM, and our proposed IWKFCM method. From a qualitative point of view we can observe that using each of the three previously available clustering methods, the segmentation result can be under-segmented (incomplete) along weak/fuzzy edges or over-segmented including disturbances causing by connected vessels, while IWKFCM achieves a better segmentation result of the nodule with more complete edge.

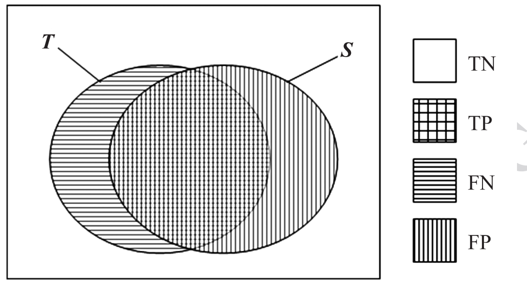

Fig. 4 Illustration of evaluation metrics for region overlapping
图 4 基于区域的分割评价示意图

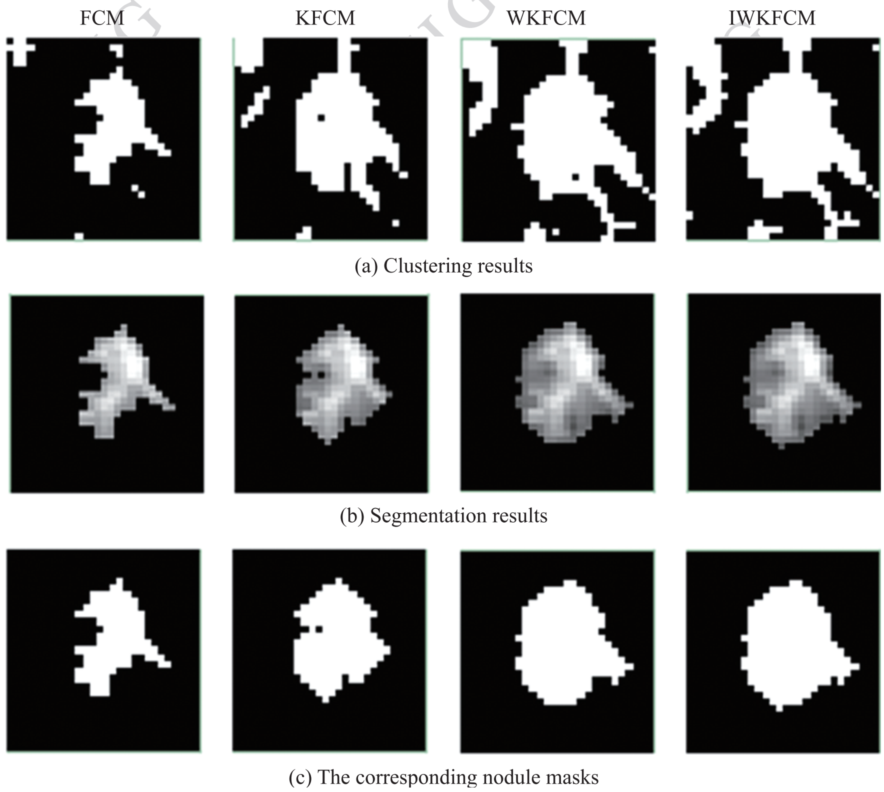

Fig. 5 Demonstration of applying four clustering segmentation algorithms one nodule area depicted on center slice including
图 5 4 种不同方法结节分割结节过程

Table 1 summaries and compares the average automated pulmonary nodule segmentation accuracy when applying FCM, KFCM, WKFCM and IWKFCM algorithms to the first clinical lung CT image dataset selected from LIDC. The results show that both average overlap ratios computed based on the entire pulmonary nodule volume and the nodule area depicted on a single center slice are gradually increased by taking steps to modify the classic FCM method. Specifically, the two computed average overlap ratios of the entire nodule volume and the nodule area depicted on the center slice are substantially increased from 45.75% and 54.87% to 76.18% and 83.96% when using FCM and IWKFCM algorithms, which represents 67% and 53% increase in the agreement between the automated and manual segmentation of entire pulmonary nodule volume and nodule area depicted on the center slice, respectively. Comparing with WKFCM, using IWKFCM also increases the average segmentation accuracy (or agreement) by 3.5% and 4.0% in computing two overlap ratios. In addition, Table 1 also shows that using IWKFCM algorithm yields the highest FPR value and smallest FNR value, which indicates that IWKFCM has highest discriminatory power in identifying pixels belonging to the nodule, during the data clustering at a cost of slightly increasing the errors of misclassifying other non-nodule pixels into nodule class.

Similar to Table 1, Table 2 summarizes and compares the average automated segmentation results when applying the four algorithms of FCM, KFCM, WKFCM, and IWKFCM to the second dataset collected from Shanghai Pulmonary Hospitals. The two computed average overlap ratios are also substantially increased from 54.45% and 70.20% to 71.65% and 84.86% when using FCM and IWKFCM, which represents 32% and 21% increase of the computed segmentation accuracy on two overlap ratios, respectively. Table 2 also shows that using IWKFCM yields the highest FPR and the smallest FNR values. However, in the busy clinical environment due to the large amount of lung CT images, this high FPR could be accepted in order to improve the efficient of segmentation.

Table 1 Comparison of average segmentation results when applying four automated algorithms to 36 sub-solid pulmonary nodules selected from LIDC datasets

表 1 临床数据集的分割结果

/%

	FCM	KFCM	WKFCM	IWKFCM
Overlap	45.75	64.05	73.58	76.18
FPR	1.74	5.50	15.41	16.33
FNR	53.30	31.98	12.38	11.55
Overlap_CS	54.87	73.36	80.76	83.96

Table 2 Comparison of average segmentation results when applying four automated algorithms to 18 sub-solid pulmonary nodules selected from CT examinations conducted in a local hospital

表 2 标准数据集的分割结果

/%

	FCM	KFCM	WKFCM	IWKFCM
Overlap	54.45	62.22	65.70	71.65
FPR	8.09	7.68	16.17	16.72
FNR	40.65	32.60	23.49	15.49
Overlap_CS	70.20	76.56	78.13	84.86

4 Discussion

In this study, considering that most currently existing segmentation methods focus on image intensity, we propose the IWKFCM method combining the intensity information and spatial structure characteristic of sub-solid nodules. Based on a similar idea, the WKFCM method present a weighting idea on general MRI-T1 image segmentation; however, there is not a clear detailed formula to define the weights in this segmentation. We choose the vessel measure function as the segmentation weights, the main reason is that for sub-solid nodule segmentation, the vessel structures make an important effect on the final segmentation result. This point also leads to the failure of most current segmentation methods on sub-solid nodule segmentation.

Then, we test our new pulmonary nodule segmentation method using a set of relatively difficult and diverse cases collected from two data sources. One is a public database (LIDC) and one is a private dataset collected from a local hospital. All nodules involved in this study are sub-solid nodules. Using these two datasets collected from two different sources also has a number of advantages. First, since performance assessment of any computerized methods depend on the difficult level of testing datasets, the segmentation results reported in this study can be objectively compared with other many previous or future studies conducted by other researchers using the same dataset (LIDC). Second, we are able to test the robustness of the algorithm using the CT images collected from different CT machines and CT data acquisition protocols. Our experimental results indicate that the proposed IWKFCM method enables to obtain more accurate results in segmenting these two sets of sub-solid pulmonary nodules than the other three previously used data clustering based segmentation methods. Although there is difference in the detailed level (degree) of performance improvement between two datasets, the performance improvement and different segmentation error (FPR and FNR) trends are consistent in two datasets. Such consistence indicates not only the improved segmentation performance but also the robust performance. In addition, we also report higher overlap ratios than the previously reported studies[10-14] in segmenting sub-solid nodules. Although the direct comparison of these reported overlap ratios is not appropriate due to the use of different testing datasets in different studies, we believe that by considering the diverse characteristic of our two testing datasets, the IWKFCM algorithm is able to achieve higher or very comparable accuracy in segmenting pulmonary nodules in particular the sub-solid nodules depicted on a diverse set of lung CT images than the existing algorithms applied to pulmonary nodule segmentation.

Comparing to the existing methods, the IWKFCM method has a number of unique advantages when applying to segment pulmonary nodules. First, it considers both the vessels structure information and the classes' distribution during segmentation. Second, it is a semi-automatic segmentation method that can be used in a busy clinical environment commendably. Third, due to its effectiveness in addressing fuzzy and uncertain problem of images, the IWKFCM method is preferable for sub-solid nodule segmentation that was less studied by scholars.

Despite the encouraging results, this is a preliminary study with a number of limitations. First, because medical images contain lots of information about focus and tissues, we still could use more adequate information involving in CT images to develop fuzzy clustering. Second, though we focus on developing practical utility segmentation for sub-solid nodules on a CAD system, the high FPR is still a problem. For these existing problems we will spend more time in our further research.

5 Conclusion

Although accurate segmentation of pulmonary nodules has significantly scientific merit in many clinical applications including lung cancer diagnosis, management of radiation therapy, and evaluation of treatment efficacy, manual segmentation of 3D pulmonary nodules depicted on multiple CT image slices is a difficult and time-consuming task. As a result, developing automated pulmonary nodule segmentation schemes (or algorithms) has been attracting extensive research interest in medical imaging and biomedical engineering related fields in the last decade. Despite great research efforts, accurately and robustly segmenting pulmonary nodules, in particular the sub-solid nodules, using computerized schemes remains a technical challenge. Based on the analysis of sub-solid nodules' characteristics, combined with the Hessian matrix eigenvalues, a 3D connected component labeling and morphological techniques, we propose and test the IWKFCM clustering method. Our experimental results show that the proposed method enables to achieve more accurate result in segmenting sub-solid pulmonary nodules than the other previously reported clustering methods. Furthermore, it can provide a consultative reference for more accurately extracting image features and optimal classification of pulmonary nodules in developing computer-aided detection (CAD) schemes.

参考文献(References)

[1] Kazerooni E A. Lung cancer screening [J]. Eur. Radiol. Suppl., 2005, 15(4):48-51.

[2] Henschke L C, Yankelevitz D F, Mirtcheva R, et al. CT screening for lung cancer: frequency and significance of part-solid and nonsolid nodules[J]. AJR, 2002, 178(5): 1053-1057.

[3] Brown M S, Goldin J G, Suh R D, et al. Lung micronodules: automated method for detection at thin-section CT-initial experience [J]. Radiology, 2003, 226(1): 256-262.

[4] Ko J P, Betke M. Chest CT: automated nodule detection and assessment of change over time-preliminary experience [J]. Radiology, 2001, 218(1): 267-273.

[5] Sluimer I, Schilham A, Prokop M, et al. Computer analysis of computed tomography scans of the lung: a survey [J]. IEEE Trans. on Med. Imaging, 2006, 25(4):385-406.

[6] Ferretti G, Félix L, Serra-Tosio G, et al. Non-solid and part-solid pulmonary nodules on CT scanning [J]. Rev. Mal. Respir., 2007, 24(10):1265-1276.

[7] Nakata M, Saeki H, Takata I, et al. Focal ground-glass opacity detected by low-dose helical CT [J]. Chest, 2002, 121(5): 1464-1467.

[8] Kostis W, Reeves A, Yankelevitz D, et al. Three-dimensional segmentation and growth-rate estimation of small pulmonary nod-

ules in helical CT images[J]. IEEE Trans. on Med. Imaging, 2003, 22 (10): 1259-1274.

[9] De Hoop B, Gietema H, van Ginneken B, et al. A comparison of six software packages for evaluation of solid lung nodules using semi-automated volumetry: what is the minimum increase in size to detect growth in repeated CT examinations[J]. European Radiology, 2009, 19: 800-808.

[10] Zhang L, Zhang T T, Novak C L, et al. A computer-based method of segmenting ground glass nodules in pulmonary CT images: comparison to expert radiologists' interpretations[C]// Proceedings of SPIE. San Diego, CA: SPIE, 2005, 5747: 113-121.

[11] Zhou J H, Chang S M, Metaxas D N, et al. Automatic detection and segmentation of ground glass opacity nodules[C]// Proceedings of MICCA Berlin: Springer, 2006(4190):784-791.

[12] Yoo Y, Shim H, Lee S U, et al. Segmentation of ground glass opacities by asymmetric multi-phase deformable model[C]//Proceedings of SPIE San Diego, CA: SPIE, 2006, 6144: 1709-1717.

[13] Browder W A. The segmentation of nonsolid pulmonary nodules in CT images [D]. Cornell: Faculty of the Graduate School of Cornell University, 2007.

[14] Tao Y, Lu L, Dewan M, et al. Multi-level ground glass nodule detection and segmentation in CT lung images[C]//Proceedings of MICCAI 2009. Berlin: Springer, 2009:715-723.

[15] Wang Q, Song, E, Jin R, et al. Segmentation of lung nodules in computed tomography images using dynamic programming and multidirection fusion techniques [J]. Academic Radiology, 2009, 16(6): 678-688.

[16] Kubota T, Jerebko A K, Dewan M, et al. Segmentation of pulmonary nodules of various densities with morphological approaches and convexity models [J]. Medical Image Analysis, 2011, 15(1): 133-154.

[17] Dehmeshki J, Amin H, Valdivieso M, et al. Segmentation of pulmonary nodules in thoracic CT Scans: a region growing approach [J]. IEEE Transactions on Medical Imaging, 2008, 27(4): 467-480.

[18] Jain A K, Murty M N, Flynn P J. Data clustering: a review [J]. ACM: Computing Surveys, 1999, 31(3): 264-323.

[19] Zhang S, Dong J W, She L H. The methodology of evaluating segmentation algorithms on medical image [J]. Journal of Image and Graphics, 2009, 14(9): 1875-1880.

[20] Liew A, Yan H. An adaptive spatial fuzzy clustering algorithm for 3-D MR image segmentation[J]. IEEE Trans. on Med. Imag., 2003, 22(9): 1063-1075.

[21] Chen S C, Zhang D Q. Robust image segmentation using FCM with spatial constraints based on new kernel-induced distance measure[J]. IEEE Trans. on Syst. Man Cybernet., 2004, 34(4):1907-1916.

[22] Bezdek J C. Pattern Recognition with Fuzzy Objective Function Algorithms [M]. New York: Springer, 1981.

[23] Zhang D Q, Chen S C. A novel kernelized fuzzy C-means algorithm with application in medical image segmentation[J]. Artificial Intelligence in Medicine, 2004, 32(1):37-50.

[24] Xue G J, Wang Y, Zhao H T, et al. Improved fuzzy kernel clustering algorithm [J]. Chin. J. Med. Imaging Technol., 2005, 21(10):1609-1611.

[25] Frangi A F, Niessen W J, Vincken K L, et al. Multiscale vessel enhancement filtering [C]//MICCAI 1496. Berlin, German: Springer Berlin Heidelberg, 1998:130-137.

[26] Rashindra M, Viergever M A, Niessen W J. Vessel enhancing diffusion: a scale space representation of vessel structures [J]. Medical Image Analysis, 2006, 10(6):815-825.

[27] Xiang S J, Li B, Tian L F, et al. Suspected lung nodule segmentation method of edge-preserving smoothing and improved FCM [J]. Computer Engineering and Applications, 2010, 46(32): 202-204.

[28] Reeves A P, Biancardi A M, Apanasovich T V, et al. The Lung Image Database Consortium (LIDC): a comparison of different size metrics for pulmonary nodule measurements [J]. Acad. Radiol., 2007, 14(12): 1475-1485.

[29] Ji Z, Xia Y, Sun Q, et al. Fuzzy Local Gaussian Mixture Model for brain MR image segmentation [J]. IEEE Transactions on Information Technology in BioMedicine, 2012, 16(3): 339-347.